Available online at www.garmian.edu.krd

Passer Journal

Passer 6 (Issue 1) (2024) 198-213

http://passer.garmian.edu.krd/

Machine Learning Models for Predicting Flexural Behavior of FRP-Strengthened RC Beams

Nasih Habeeb Askander[1*]

[1]*Civil Engineering Department, University of Halabja, Kurdistan Region – Iraq,*

Received 14 January 2024; revised 23 March 2024;
accepted 23 March 2024; available online 02 May 2024

DOI: 10.24271/PSR.2024.435650.1472

ABSTRACT

This study's objective is to overcome limitations in current design recommendations by exploring the application of machine learning to predict the flexural behavior of fiber-reinforced polymer (FRP)-strengthened reinforced concrete beams. Although FRP composites have completely changed structural strengthening, it might be challenging to predict bending moments with precision. This work fills the theoretical and experimental findings gaps by utilizing Artificial Neural Network (ANN) models in conjunction with computational techniques and statistical analysis. It includes gathering data, conducting a thorough literature review, and developing three models: Artificial neural network (ANN), Non-linear Regression (NLR), and Linear Regression (LR). Despite other models, the ANN model stands out for its superior performance and accurate predictions. Understanding material characteristics, FRP properties, and beam dimensions is critical in predicting flexural strength. The most significant parameter studied in this research is the overall depth of the beam (h), followed by the variation in bottom flexural reinforcement (ρ_s). Additionally, the FRP ratio (ρ_f) and beam width (b), which are both regarded as significant attributes, influence the flexural capacity of FRP-strengthened beams. The ultimate moment (M_u) may be predicted by the ANN model with an error range of -20% to +15%, indicating a significant advancement in strengthening approach optimization. This development could reduce the requirement for expensive experimental testing during construction, thereby enhancing the predictive capacity of structural engineering procedures. Furthermore, the design of flexurally strengthened RC beams with FRP may be made possible by depending on this model, specifically the ANN, without the need for experimental effort.

Keywords: RC beam, Strengthening, FRP,Modeling, ANN.

1. Introduction

Composites made of FRP have completely altered the method by which concrete constructions are strengthened. They provide improved load-bearing capacities, fulfill inaccurate code requirements, and repair environmental damage[1-4]. Over the past few decades, many experimental and theoretical studies have examined the behavior of reinforced concrete (RC) structures strengthened by various techniques, such as externally bonded fiber-reinforced polymer (EB-FRP) and near-surface mounted FRP (NSM-FRP)[5-12].

The ultimate bending moments in strengthened beams are often predicted in the context of design standards using common assumptions. Even though those predictions are well supported by research, they frequently fail to accurately describe the real performance of strengthened beams. That is because they mostly rely on ideas about the failure of tension reinforcement or the collapse of the concrete compression zone, ignoring the wide range of factors that can affect real performance[13].

In structural engineering, machine learning (ML) deals with tasks like damage detection and strength predictions. It includes supervised, unsupervised, and reinforcement learning. Neural networks, decision trees, support vector machines, and other algorithms are commonly utilized. In engineering design, the utilization of surrogate models, alternatively termed metamodels, serves to mitigate computational complexity by simplifying intricate machine-learning models. Because of its adaptability, machine learning (ML) provides engineers with useful insights that improve the efficiency and accuracy of operations related to the design, analysis, and maintenance of civil infrastructure. By facilitating well-informed decision-making and optimization, these methods help to develop resilient and sustainable infrastructure systems[14].

Artificial neural networks (ANN) encompass various types, including the commonly known neural networks (NN). Typically, a neural network (NN) has input, hidden, and output layers. Neurons use weights to determine which information to send to the next layer. The back propagation (BP) algorithm uses gradient descent to modify neuron weights during training. In an artificial neural network (ANN), neurons cycle, and information spreads

* Corresponding author
E-mail address: nasih.askandar@uoh.edu.iq (Instructor).
Peer-reviewed under the responsibility of the University of Garmian.

throughout the network. The BP algorithm improves the network's information processing capacity by optimizing neuron weights during training[15, 16].

Since FRP laminate is lightweight, non-corrosive, and effective at strengthening and repairing seismic structures, it offers a viable alternative for use as a strengthening component in concrete structures. Investigations have, however, revealed certain difficulties, such as the composites' tendency to debond from concrete surfaces before they achieve the laminates' rupture strength. As a solution to these issues, research into ANN models for structural behavior prediction has garnered interest[17]. The goal of this study is to predict the ultimate load capacity of reinforced concrete beams strengthened with FRP using multi-layer perceptron neural networks and backpropagation algorithms. A comprehensive parametric study is performed to understand and improve the performance of concrete beams strengthened using FRP.

Based on the American Concrete Institute guideline (ACI 440.2R-08)[18] recommendations, Xue et al.[19] used theoretical frameworks to demonstrate that there was a significant gap between experimental data and theoretical predictions for strengthening RC beams using prestressed carbon fiber-reinforced polymer plates, this illustrated the drawbacks of these methodologies. *Mahmoud et al.*[20] revealed flaws in the method of predicting ultimate bending moments for RC beams utilizing Near Surface Mounted Fiber Reinforced Polymer (NSM-FRP), which further illustrated the necessity for more precise estimation methods. This study suggests a novel approach to fill this gap by estimating the bending moments of reinforced beams using ANN models. In civil engineering applications, ANNs are frequently employed as a tool for a variety of operations, including structural assessments, and shear strength prediction in FRP-strengthened RC elements[13, 17, 21, 22]. The implementation of AI-based predictive maintenance systems for civil infrastructure is a possible area of future research. Such advancements can involve developing algorithms to evaluate monitoring data and predict probable structural degradation or equipment failures, enabling proactive maintenance treatments and better asset management techniques.

In 1997, data provided by *Arduini M. and Nannin* presented samples of RC beams strengthened with sheets of carbon fiber-reinforced polymer (CFRP). CFRP was utilized to strengthen the surface of the concrete. Several variables were examined, including load locations, surface preparation, and CFRP configurations. Some variables had a negligible influence, but the strengthening effect was substantial[23].

The behaviors of bonded FRP-strengthened RC beams were investigated in 2001 by *Rahim H. and Hutchinson A.*, flexural tests on 2.3m concrete beams with externally bonded reinforcements, as well as variations in the kind and amount of internal reinforcement, were conducted as part of the experimentation. For comparison, bonded steel plates were used in certain beams. A 2D non-linear finite-element model for concrete with a "damaged" material model was integrated into the theoretical investigation. The experimental results generally demonstrated good correlations with models of non-linear finite elements[24].

The goal of a 2001 study by *Brena SF et al*. was to employ CFRP composites to raise the flexural capacity of bridges. During the initial phase, four CFRP systems were used to test twenty-two concrete beams, and designs to avoid early debonding were investigated. Following fatigue tests on eight beams, it was found that there was no interface degradation under one million cycles; nevertheless, the analytical model was unable to simulate material strains resulting from CFRP debonding[25].

The load capacity of RC beams with the same deformational resemblance to reference beams was enhanced in 2005 by *Barros JAO and Fortes AS* applying CFRP laminate strips to conduct the near-surface mounted (NSM) technique. implementing this technique, the CFRP acquired 62%–91% of its ultimate strain, significantly increasing both the load at the serviceability limit and stiffness after cracking. In strengthened RC beams, load-carrying capability, and deflection were precisely predicted by numerical modeling[26].

The use of CFRP rods in NSM-strengthening concrete structural components was investigated by *Al-Mahmoud et al.* in 2009. Using carbon-epoxy pultruded FRP rods with a diameter of 6 and 12 mm. Their study examined the overall performance of NSM-strengthened RC beams under flexure. Various vibrated concrete compositions (regular VC30 and high-strength VC60) and filler materials (mortar and resin) were tested up to the failure load. Test results compared to current analytical models confirmed that adding NSM reinforcement to concrete structural elements provided outstanding outcomes[20].

Twenty concrete beams strengthened with NSM-FRP bars were investigated by *Soliman S. and El-Salakawy* in 2010, evaluating the diameter, bonding, steel ratio, kind of bar, and size of the groove. The results show how well NSM-FRP increases the beams' flexural strength. Furthermore, the outcomes of experiments are successfully mirrored by 3D finite element analysis, which demonstrates strong agreement in the areas of failure modes, ultimate capacity, load-deflection, and strain[27].

To increase the flexural strength of concrete, Nakul (2012) studied the application of NSM-CFRP or CFRP strips. Due to its advantages over external CFRP laminates in terms of strength, stiffness, bonding, adjacent member anchoring, and simplicity of installation, NSM-CFRP has attracted attention from structural engineers worldwide. Under static or impact loads, this investigation assessed NSM-CFRP retrofits in RC beams and slabs. It found notable increases in strength and stiffness, especially in impact resistance, with possible applications in a variety of structures[28].

The four-point bending RC beams reinforced with NSM FRP bars were examined in the 2014 study by Sharaky et al. Material type, epoxy characteristics, bar size, and the quantity of NSM bars were among the variables examined. The results of the analysis demonstrated significant load improvements for CFRP and GFRP (155.8% and 129.8% in yielding loads and 166.3% and 159.4% in ultimate loads). Variations in epoxy and bar had a negligible impact on load capacity; failures in epoxy or concrete cover delamination occurred[29].

In Al-Obaidi's 2015 project, various retrofitting techniques for structural modifications, such as the use of steel plates and FRP jackets, were examined to improve shear and flexural

capabilities. Although FRP has advantages, there were corrosion issues. The study concentrated on NSM-CFRP rods, analyzing their bond properties using pullout testing and evaluating how well they worked as reinforcing elements for concrete beams[30].

A study in 2016 by *Seo et al.* examined how partially debonded NSM-FRP strips of various lengths potentially increase the RC beams' bending strength. To increase the bonded surface without changing the FRP area, they concentrated on the impact of the de-bonded region's placement within the FRP strip. By applying the current equations to evaluate the flexural strength, the study discovered that the deformation capacity increased when a de-bonded zone was positioned in the center, allowing for a uniform distribution of FRP strain. Triple lines of NSM FRP strips were used, which resulted in stronger bonds due to higher anchorage strength[31].

In their 2017 work, *Daghash SM and Ozbulut OE* examined RC beams strengthened with NSM basalt fiber-reinforced polymer bars. For a bond failure model to be relevant, independent of the CFRP reinforcement's geometry, they evaluated the effects of NSM BFRP bars on restoring capacity and improving ductility while at the expense of smaller deflection capacity by testing five 2100mm beams with different reinforcement ratios. They conducted this by using strain gauges, digital image correlation, and four-point bending tests[32].

An equivalent section model proposed by *Woo et al.* (2017) assumed that the CFRP reinforcement and filler would behave in a unified manner. The bond failure model that was generated was evaluated analytically and verified by experiments conducted on NSM CFRP-reinforced beams with varying cross-sections. The exact failure mechanism prediction and accurate correlation with experimental data were demonstrated to be achievable, irrespective of the geometry of the CFRP reinforcement[33].

To evaluate their effect on beam response, *Trung et al.* tested the influence of carbon fiber strand (CFS) strengthening on RC beams in 2018. They examined displacement characteristics, response force, and crack patterns, providing a full account of the experimental techniques. Their numerical analysis produced simulated results that were in agreement with experiments by using reliable constitutive models and beam contact conditions. CFS strengthening enhanced the flexural capacity of RC beams under impact and static loads[34].

In 2020, Moawad examined the long-term and residual flexural strength of CFRP-stripped NSM-reinforced RC beams under continuous stress. Two batches of concrete with different compressive strengths were used in the study for constructing twenty-eight RC beams that were split up into Series A and B. A1 and A2 groups comprised series A, and B was further classified into B1, B2, and B3. Beams in the first group of each series were tested after 55 days to assess the short-term flexural behavior of strengthened and un-strengthened beams; the succeeding groups underwent various long-term tests[35].

Using CFRP and engineered cementitious composite (ECC), *Liu et al.* in 2023 focused on enhancing the RC beam's flexural strength. The experimental study verified that the use of CFRP alone caused early delamination; however, this can be avoided by combining CFRP with ECC. The composite approach led to considerable improvements in energy absorption, stiffness, ductility, and load capacities (up to 23–31% for cracking load). When the projected and tested flexural bearing capacities were compared, the prediction model showed excellent accuracy, with error variations within 5%[36].

The ANN is a computational method for addressing problems that may produce definitive findings with little time and expense. It mimics the human brain's capacity to learn from the past and make predictions. In the discipline of structural engineering, ANN has gained popularity recently, particularly in identifying relationships in data.

This study looks at the theory of flexure in reinforced concrete beams reinforced with FRP and then analyses the guidelines that are already in place for this kind of research. Next, by creating prediction models and using data from relevant studies in the field of FRP-strengthened RC beams, the correspondence between input and output data is developed to ascertain the ultimate flexural strength.

Additionally, the soft computing techniques utilized for predicting Mu for enhanced RC beam properties have limits. Hoang et al.[13] evaluated the Mu of strengthened RC beams using an ANN model. They combined 131 investigation results with six input parameters identified in the literature to produce the ANN models. They concluded that applying an ANN model to predict the Mu of a strengthened RC beam using FRP fiber is an effective strategy[13].

This comprehensive investigation integrates computational approaches, artificial neural networks, and machine learning techniques to solve significant challenges in flexural strength prediction and strengthening technique optimization for improved structural performance in FRP-strengthened concrete beams. The study offers a substantial contribution to the development of structural engineering techniques by trying to fill the gap between theoretical predictions and experimental results. Due to a lack of research on the creation of different models, this study was conducted to estimate the flexural strength of a strengthened RC beam using three different models and six input factors.

2. Research Significance

This research is important because it takes a novel approach to overcoming shortcomings with the design guidelines that are already in place for RC beams strengthened using FRP. This work fills theoretical and experimental gaps in the prediction of flexural behavior by utilizing machine learning, namely ANN models, in conjunction with computational methods and statistical analysis. A significant achievement in enhancing strengthening is provided by the ANN model's exceptional performance and accuracy. This discovery could significantly reduce the need for expensive experimental testing. In the end, this development opens the door for more accurate and efficient structural engineering processes, which will enable the design of flexural strengthened RC beams using FRP without requiring much experimental work.

3. Flexural Strength of RC of FRP-strengthened RC beams

A rectangular section in flexure at the state of ultimate limit is demonstrated in Figure 1 with internal strain and stress distribution.

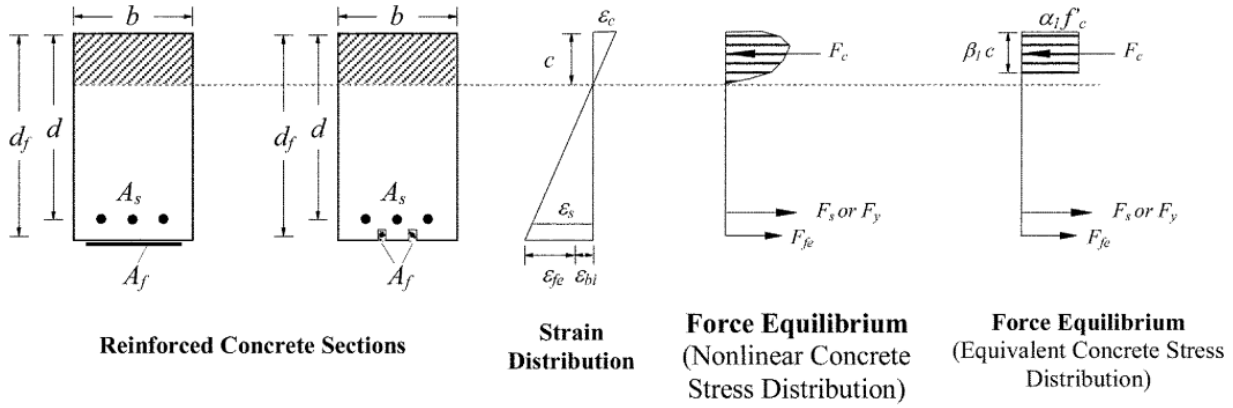

Figure 1: strain and stress distribution at the ultimate limit state for a rectangular section in flexure[37].

Equation one determines the section's nominal flexural strength with FRP external reinforcement. An extra reduction factor, φ_f, further diminishes the flexural-strength contribution of the FRP reinforcement. The recommended value φ_f is 0.85[37, 38].

$$M_n = A_s f_s \left(d - \frac{\beta_1 c}{2}\right) + \varphi_f A_f f_{fe} \left(d_f - \frac{\beta_1 c}{2}\right) \quad (1)$$

Based on the design model in the ACI 440.2R-17[37],

$$f_s = E_s \varepsilon_s \leq f_y \quad (2)$$

Equations 3 and 4 can be used to compute the strain in the concrete and the reinforcing steel using identical triangles. $\varepsilon_s = \left(\varepsilon_{fe} + \varepsilon_{bi}\right)\left(\frac{d-c}{d_f-c}\right)$ (3)

$$\varepsilon_c = \left(\varepsilon_{fe} + \varepsilon_{bi}\right)\left(\frac{c}{d_f-c}\right) \quad (4)$$

Utilizing ACI 318-05, concrete stress block factors can be computed[39]. The parabolic stress-strain relationship for concrete can also be used to approximate stress block factors, as seen below:

$$\beta_1 = \frac{4\varepsilon'_c - \varepsilon_c}{6\varepsilon'_c - 2\varepsilon_c} \quad (5)$$

$$\alpha_1 = \frac{3\varepsilon'_c \varepsilon_c - \varepsilon_c^2}{3\beta_1 {\varepsilon'_c}^2} \quad (6)$$

$$\varepsilon'_c = \frac{1.7 f'_c}{E_c} \quad (7)$$

$$c = \frac{A_s f_s + A_f f_{fe}}{\alpha_1 f'_c \beta_1 b} \quad (8)$$

$$f_{fe} = E_f \varepsilon_{fe} \quad (9)$$

$$\varepsilon_{fe} = 0.003\left(\frac{d_f - c}{c}\right) - \varepsilon_{bi} \leq \varepsilon_{fd} \quad (10)$$

$$\varepsilon_{bi} = \frac{M_{DL}(f_f - kd)}{I_{cr} E_c} \quad (12)$$

$$k = \sqrt{\left(\rho_s \frac{E_s}{E_c} + \rho_f \frac{E_f}{E_c}\right)^2 + \left(\rho_s \frac{E_s}{E_c} + \rho_f \frac{E_f}{E_c}\left(\frac{d_f}{d}\right)\right)} - \left(\rho_s \frac{E_s}{E_c} + \rho_f \frac{E_f}{E_c}\right) \quad (13)$$

$$\varepsilon_{fd} = 0.41\sqrt{\frac{f'_c}{n E_f t_f}} \leq 0.9\varepsilon_{fu} \quad (14)$$

$$\rho_f = \frac{n b_f t_f}{bh} \quad (15)$$

All the variables used in the equations stated above are included in Table 1. The features of the FRP sheets, such as the modulus of elasticity, which can vary depending on the kind of GFRP or CFRP, sheet thickness, effective width, and number of layers, have significant effects on flexural strength.

Table 1: Flexural strength Effective parameters for FRP-strengthened RC beams.

Parameters	
Width of reinforced concrete beam	*b (mm)*
Height of reinforced concrete beam	*h (mm)*
Compressive strength of concrete	*f'c (MPa)*
Flexural reinforcement ratio	*ρ_s (%)*
FRP ratio	*ρ_f (%)*
The FRP sheet's modulus of elasticity	*E_{frp} (MPa)*

The selection criteria and rationale for these input parameters originate from their direct impact on the flexural strength of FRP-strengthened RC beams, as well as their extensive use in structural analysis and design:

I. The width (*b*) and height (*h*) of an RC beam: The structural behavior and capacity of an RC beam are directly influenced by its dimensions. The basic geometric parameters of width and

height have an impact on how stresses and strains are distributed throughout the beam.

II. Concrete compressive strength ($f'c$): The RC beam's ability to withstand compression forces is determined by the concrete's compressive strength, which is an important parameter. In general, higher compressive strength equals higher beam capacity.

III. Flexural reinforcement ratio (ρ_s): The quantity of flexural reinforcement influences the beam's resistance to shear and bending forces. A larger reinforcement ratio increases the beam's ability to sustain flexural loads.

IV. FRP ratio (ρ_f): The beam's flexural behavior and capacity are influenced by the ratio of FRP reinforcement used in it. Usually, Increasing the FRP ratio results in a stronger, more rigid beam.

V. Elastic modulus of FRP (E_{frp}): The stiffness and deformation properties of the beam are influenced by the modulus of elasticity of the FRP material that is used for reinforcement. A beam with a higher modulus of elasticity is stiffer and has less deflection when under load.

These parameters are crucial for creating accurate predictive models since they together capture the main elements influencing the behavior of the beams.

4. Methodology and Models

4.1 Data Collection

For this study, 136 datasets from various literature sources were gathered and organized into an Excel sheet. After that, the data were divided into three groups, statistical examination was done, and random sorting was performed. Models were created using the training dataset, which was the largest piece of data and made up 70% of the total data. The remaining two groups were used to test and validate the models; they accounted for 15% of the datasets each[13, 40, 41]. The variables database for each sample are summarized in Table 2.

Earlier research evaluating the impact of FRP sheets upon flexural strength was found through the authors' searches. The input dataset is shown in Table 2 and includes i. the RC beam's width (b); ii. its height (h); iii. the concrete's compressive strength ($f'c$); iv. the flexural reinforcement ratio (ρ_s); v. the FRP ratio (ρ_f); vi. its modulus of elasticity (E_{frp}).

Using the dataset that was provided, which comprised the six independent components previously mentioned, the enhanced RC beam's flexural strength was estimated. The aim is to minimize the number of laboratory test batches required to quickly optimize the number of components for a specific Mu by utilizing all of the mentioned input variables. The methodology for this experiment is explained in Figure 2.

Table 2: Statistical specifications of input data.

no.	Authors	Strengthened technique	Strengthened Material	Label	b (mm)	h (mm)	f'c (Mpa)	ρ_s (%)	ρ_f (%)	E_{frp} (Gpa)
1	Arduini and Nanni [23]	Externally bonded system	CFRP	SM2	320	160	36	0.642	0.332	235
2				SM3	320	160	36	0.642	0.332	235
3				SM4	320	160	36	0.642	0.332	235
4				SM5	320	160	36	0.642	0.332	235
5				SM6	320	160	36	0.642	0.332	235
6				ST2	320	160	36	0.642	0.332	235
7				ST3	320	160	36	0.642	0.332	235
8				ST4	320	160	36	0.642	0.332	235
9				MM2	160	320	36	0.931	0.135	235
10				MM3	160	320	36	0.931	0.135	235
11				MM4	160	320	36	0.931	0.135	235
12				MT2	160	320	36	0.931	0.135	235
13				MT3	160	320	36	0.931	0.135	235
14				MT4	160	320	36	0.931	0.135	235
15				MT5	160	320	36	0.931	0.135	235
16	Rahim H and Hutchinson A. [24]	Externally bonded system		A4	200	150	50	0.433	0.517	127
17				A5	200	150	50	0.433	0.517	127
18				A6	200	150	50	0.433	0.776	127
19				A7	200	150	50	0.433	0.776	127
20				A8	200	150	50	0.433	0.517	127
21				A9	200	150	50	0.433	0.517	127
22				A10	200	150	50	0.433	0.517	127
23				A11	200	150	50	0.433	0.517	127

24				B3	200	150	50	0.683	0.261	127
25				B4	200	150	50	0.683	0.261	127
26				B5	200	150	50	0.683	0.783	127
27				B6	200	150	50	0.683	0.783	127
28				B7	200	150	50	0.683	1.174	36
29				B8	200	150	50	0.683	1.174	36
30				C3	200	150	50	0.903	0.268	127
31				C4	200	150	50	0.903	0.268	127
32				C5	200	150	50	0.903	0.804	127
33				C6	200	150	50	0.903	0.804	127
34				C7	200	150	50	0.903	1.205	36
35				C8	200	150	50	0.903	1.205	36
36	Brena SF et al. [25]	Externally bonded system	CFRP	A1	203	356	35.1	0.62	0.100	227.5
37				A2	203	356	35.1	0.62	0.100	227.5
38				A3	203	356	35.1	0.62	0.100	227.5
39				A4	203	356	35.1	0.62	0.200	227.5
40				B1	203	356	37.2	0.62	0.150	230.3
41				C1	203	406	35.1	0.62	0.082	62.1
42				C2	203	406	35.1	0.62	0.082	62.1
43				D1	203	406	37.2	0.62	0.094	155.1
44				D2	203	406	37.2	0.62	0.094	155.1
45	Barros JAO and Fortes AS [26]	NSM	CFRP	V1R1	100	170	45.3	0.368	1.130	158.8
46				V2R2	100	177	48.9	0.551	0.260	158.8
47				V3R2	100	175	42.8	0.699	0.261	158.8
48				V4R3	100	180	46.4	0.986	0.392	158.8
49	Al-Mahmoud et al. [20]	NSM	CFRP	S-C 6 (VC30)	150	280	37.5	0.745	0.158	145.9
50				S-C 6 (270-R)	150	280	36.5	0.745	0.158	145.9
51				S-C6 (210-R)	150	280	36.7	0.745	0.158	145.9
52				S-C 12 (VC30)	150	280	35.1	0.745	0.317	145.9
53				S-C 12 (VC60)	150	280	67.2	0.745	0.317	145.9
54				S-C6 (VC60)	150	280	66.5	0.745	0.158	145.9
55				S-C6 (270-M)	150	280	38.1	0.745	0.158	145.9
56	Soliman S and El-Salakawy [27]	NSM		A1	200	300	35	1.553	0.137	124
57				A2	200	300	35	1.553	0.137	124
58				A3	200	300	35	1.553	0.137	124
59				A4	200	300	35	1.553	0.137	124
60				B1	200	300	35	0.777	0.137	124
61				B2	200	300	35	0.777	0.137	124
62				C1	200	300	35	0.388	0.137	124
63				C2	200	300	35	0.388	0.137	124
64				C3	200	300	35	0.388	0.137	124
65				C4	200	300	35	0.388	0.137	124
66				C5	200	300	35	0.388	0.137	124
67				C6	200	300	35	0.388	0.137	124
68				C7	200	300	35	0.388	0.137	124
69				C8	200	300	35	0.388	0.246	134
70				C9	200	300	35	0.388	0.246	134
71				C10	200	300	35	0.388	0.246	45
72				C11	200	300	35	0.388	0.246	45
73	Nakul [28]	NSM	CFRP	1	152	229	34.5	0.701	0.337	137.9
74				3	152	229	34.5	0.701	0.225	137.9
75				4	152	229	34.5	0.701	0.450	137.9
76				5	152	229	34.5	0.701	0.225	137.9
77				6	152	229	34.5	0.701	0.337	137.9
78				7	152	229	34.5	0.701	0.450	137.9
79				8	152	229	34.5	1.401	0.225	137.9
80				9	152	229	34.5	1.401	0.337	137.9

81				10	152	229	34.5	1.401	0.450	137.9
82				12	152	229	34.5	1.401	0.225	137.9
83				13	152	229	34.5	1.401	0.337	137.9
84				14	152	229	34.5	1.401	0.450	137.9
85				17	152	229	34.5	2.102	0.562	137.9
86				19	152	229	34.5	2.102	0.225	137.9
87				21	152	229	34.5	2.102	0.45	137.9
88	Sharaky et al. [29]	NSM	CFRP	LB1C1	160	280	32.4	0.579	0.129	170
89			GFRP	LB1G1	160	280	32.4	0.579	0.129	64
90			CFRP	LB2C1	160	280	32.4	0.579	0.257	170
91			GFRP	LB2G1	160	280	32.4	0.579	0.257	64
92			CFRP	LA2C1	160	280	32.4	0.579	0.257	170
93			GFRP	LA2G1	160	280	32.4	0.579	0.257	64
94			GFRP	LB1G2	160	280	32.4	0.579	0.290	64
95	Al-Obaidi [30]	NSM	CFRP	AR2	165	254	29	0.732	0.183	124.1
96				AR3	165	254	30.1	0.732	0.412	124.1
97				AR4	165	254	27.6	0.732	0.732	124.1
98				AR4-S	165	254	31.7	0.732	0.366	124.1
99				BR2	165	254	30	0.412	0.183	124.1
100				BR3	165	254	32.2	0.412	0.412	124.1
101				BR4	165	254	30.3	0.412	0.732	124.1
102	Seo et al. [31]		CFRP	BP1600	200	400	21	0.43	0.082	160
103				CP1600-1	200	400	21	0.43	0.079	160
104				CP1600-3	200	400	21	0.43	0.079	160
105				CP500-1	200	400	21	0.43	0.079	160
106				CP500-3	200	400	21	0.43	0.079	160
107				CP400-1	200	400	21	0.43	0.079	160
108				CP400-3	200	400	21	0.43	0.079	160
109				CP300-1	200	400	21	0.43	0.079	160
110				CP300-3	200	400	21	0.43	0.079	160
111	Daghash SM and Ozbulut OE [32]	NSM	BFRP	S3B1	150	300	38	0.873	0.182	44.3
112				S3B2	150	300	38	0.873	0.365	44.3
113				S2B1	150	300	38	0.582	0.182	44.3
114				S2B2	150	300	38	0.582	0.365	44.3
115	Woo et al. [33]	NSM	CFRP	R-PL-15	200	300	31.3	0.412	0.040	167.0
116				R-PL-25	200	300	31.3	0.412	0.067	167.0
117				R-RD-9	200	300	31.3	0.412	0.122	121.4
118				R-PL-25*2-S	200	300	31.3	0.412	0.135	167.0
119				R-PL-25*2-2S	200	300	31.3	0.412	0.135	167.0
120				R-PD-9*2-S	200	300	31.3	0.412	0.245	121.4
121				R-PD-9*2-2S	200	300	31.3	0.412	0.246	121.4
122	Trung et al. [34]	NSM	CFRP	SR48-1	200	300	35.8	1.146	0.088	237
123				SR48-2	200	300	35.8	1.146	0.088	237
124				SR72-1	200	300	35.8	1.146	0.132	237
125				SR72-2	200	300	35.8	1.146	0.132	237
126	Moawad [35]	NSM	CFRP	AS1sh	140	180	36.0	0.769	0.137	160.9
127				AD1sh	140	180	36.0	0.769	0.274	158.3
128				AS2sh	140	180	36.0	1.967	0.137	160.9
129				AS3sh	140	180	36.8	0.769	0.137	160.9
130				BT3sh	140	180	36.8	0.769	0.411	158.3
131				BS3sh	140	180	36.8	0.769	0.137	160.9
132	Liu, D., et al. [36]	Externally bonded	CFRP	CP-1	150	250	45.2	2.04	0.53	160
133				CP-2	150	250	45.2	2.04	0.53	160
134				E30-CP-T	150	250	45.2	2.04	0.53	160
135				E30-CP-M	150	250	45.2	2.04	0.5	160
136				E30-CP-B	150	250	45.2	2.04	0.47	160

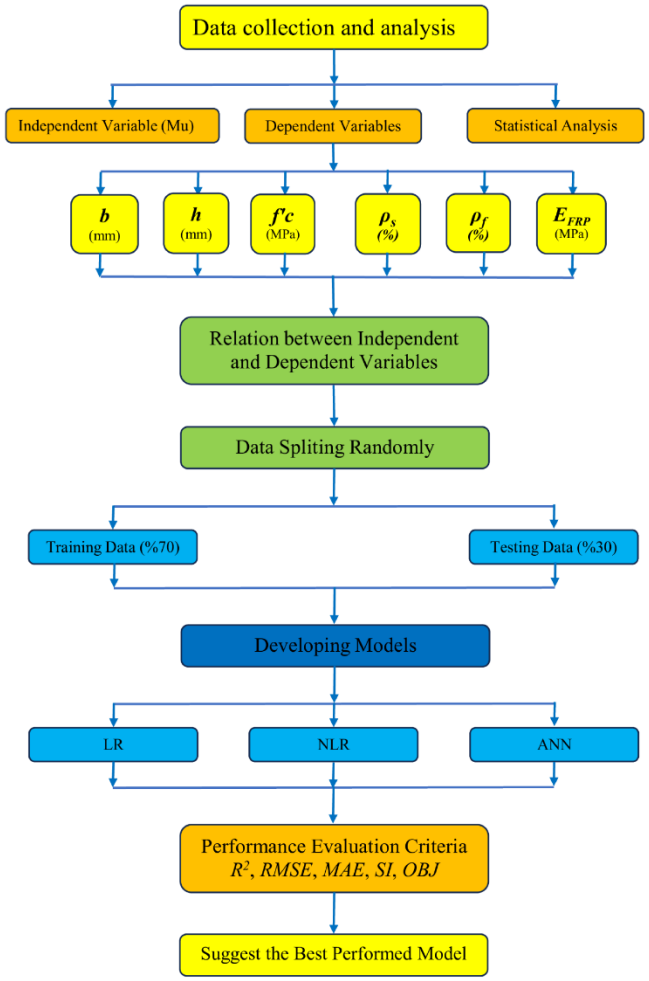

Figure 2: The flowchart diagram process followed in this study.

4.2 Modeling

It is impossible to draw a direct relation between experimental $M_{u,\,exp.}$ and predicted $M_{u,\,pred}$. According to the results of the data analysis in the following section, six input variables are employed to measure the impact of each parameter on M_u. Three distinct soft computing approaches are offered, as shown below.

4.2.1 Linear Relationship Model

As said earlier, the objective of this study is to create a model that assesses the impact of the greatest possible number of parameters on the M_u of a strengthened RC beam. Equation (16) illustrates the use of linear regression as a general technique for evaluating M_u:

$$M_u = \alpha_1 + \alpha_2(\rho_f) \quad \ldots\ldots \quad .(16)$$

Where α_1 and α_2 represent the model's inputs for ultimate flexural strength (M_u) and FRP-strengthened ratio (ρ_f), respectively. Despite their impact on M_u, beam width and other elements and variables adjusted with M_u, which are not considered in the prior model. Using the EXCEL program and a solver, the values of each parameter in the current model were determined using the least squares approach and the sum of error squares. To provide more reliable scientific data Equation (17) is proposed, which incorporates all potential influences on Mu[42].

$$M_u = \alpha_1 + \alpha_2(b) + \alpha_3(h) + \alpha_4(f_c') + \alpha_5(\rho_s) + \alpha_6(\rho_f) + \alpha_7(E_{FRP}) \quad (17)$$

Here, b stands for RC beam's width (mm), h for its height (mm), ($f'c$) is the compressive strength of the concrete (MPa), (ρ_s) is the internal steel reinforcement ratio (%), (ρ_f) is the external FRP-strengthened ratio (%), and E_{frp} stands for the elasticity modulus of the FRP sheet (MPa).

The model's parameters are $\alpha_1, \alpha_2, \alpha_3, \alpha_4, \alpha_5, \alpha_6, and\ \alpha_7$. Equation (17) can be used to expand Equation (16) since all factors can be altered linearly. M_u may be influenced by a variety of elements that engage in conversation with one another. To exactly predict the flexural strength, regular updates are required for the model.

4.2.2 Non-linear Model

Equation (18) can be used to create an NLR model [42]. Equation (1) can be used to predict the M_u by stating the relationship between the various components in Equations (16) and (17).

$$M_u = \alpha_1 \times (b)^{\alpha_2} \times (h)^{\alpha_3} \times (f_c')^{\alpha_4} \times (\rho_s)^{\alpha_5} \times (\rho_f)^{\alpha_6} \times (E_{FRP})^{\alpha_7} + \alpha_8 \times (b)^{\alpha_9} \times (h)^{\alpha_{10}} \times (f_c')^{\alpha_{11}} \times (\rho_s)^{\alpha_{12}} \times (\rho_f)^{\alpha_{13}} \times (E_{FRP})^{\alpha_{14}} \quad (18)$$

The NLR model's parameters are the same as those that were previously established. Additionally, in a similar way to the LR model, the values of each parameter were found using the least squares method and the sum of error squares using the EXCEL application and a solver.

4.2.3 ANN Model

The opposite of feed-forward neural networks is an ANN[42]. These networks consist of three different layers: input, output, and hidden layers. The hidden layer (or layers) sits between the input and output levels, letting data pass from one to the other. The input layer is responsible for receiving input data, while the output layer makes predictions and categorizes data. Trial cycles demonstrate that the number of hidden layers is variable and may be changed to improve the functionality of the model. The study's authors examined several variables, such as the number of hidden layers, neurons, momentum, learning rate, and iterations, to determine the optimal system architecture. For the current investigation, it was found that the maximum efficiency was achieved when the ANN comprised one hidden layer, eight neurons (as shown in Figure 3), 2000 iterations, a learning rate of 0.2, and a momentum of 0.1. These settings produced the highest R^2 value and the lowest MAE and RMSE values. Equations (19)–(21)[42-45] provide the equations for the ANN model. Based on the model's R^2, MAE, and RMSE performances, determine which hidden layer and neurons are optimal for an ANN model, as stated in Table 3.

Hyperparameter tuning plays a crucial role in our application of ANN to the simulation of the flexural strength of beams strengthened with FRP. We understand that ensuring the versatility and reliability of our generated models requires a clear description of our hyperparameter tuning technique.

We carefully tuned the hyperparameters in our study to maximize the effectiveness of the ANN models. We used a methodical strategy that made use of the features provided by the Weka program, which provides a range of hyperparameter optimization methods. To be more precise, we used the Weka framework in conjunction with grid search and random search techniques to thoroughly investigate the hyperparameter space.

We established ranges for important hyperparameters, including learning rates, batch sizes, and the number of hidden layers and units throughout the hyperparameter tuning procedure. The performance of the ANN models was then methodically assessed across these hyperparameter settings using evaluates like R-squared or mean squared error (MSE).

We obtained robust estimates of model performance over a range of hyperparameter settings by splitting the dataset into many subsets and iteratively training and testing the models on different subsets.

Clarity and reproducibility were our primary concerns during the hyperparameter tuning process, and we kept careful records of every action we took along with the reasoning behind it. Through this painstaking process, readers can learn more about the validity and applicability of the ANN models we created for predicting the flexural strength of FRP-strengthened beams.

From linear node 0:

$$T_u = Threshold + \left(\frac{Node\ 1}{1+e^{-B1}}\right) + \left(\frac{Node\ 2}{1+e^{-B2}}\right) + \cdots \quad (19)$$

From sigmoid node 1:

$$B1 = Threshold + \sum(Attribute \times Variable) \quad (20)$$

From sigmoid node 2:

$$B2 = Threshold + \sum(Attribute \times Variable) \quad (21)$$

Objective

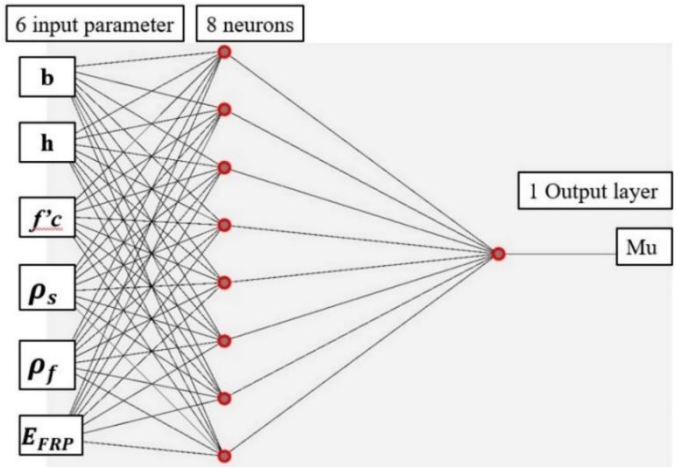

Figure 3: ANN model optimal network architecture.

Table 3: ANN designs put to the test.

Hidden layers number	no. of Neurons	R^2	MAE (MPa)	RMSE (MPa)	Hidden layers number	no of Neurons	R^2	MAE (MPa)	RMSE (MPa)
1	1	0.9344	6.40	8.10	5	1	0.9542	5.16	6.74
2	1	0.9335	6.54	8.27	5	2	0.9730	4.43	5.60
3	1	0.6991	18.53	24.28	5	3	0.9741	4.55	5.70
2	1	0.9331	5.01	6.68	5	4	0.9697	5.13	6.47
2	2	0.9509	5.15	6.95	6	2	0.9691	4.53	5.78
2	3	0.9510	5.15	6.95	6	5	0.9695	4.51	5.82
3	1	0.9514	5.12	6.83	6	7	0.9700	4.63	6.06
3	2	0.9506	5.11	6.94	7	1	0.9738	3.74	5.01
4	1	0.9659	4.82	6.07	7	2	0.9722	4.55	5.87
4	2	0.9617	4.93	6.31	7	3	0.9720	4.47	5.64
4	3	0.9630	4.99	6.39	***8***	***1***	***0.9748***	***3.68***	***4.91***
4	4	0.9640	4.95	6.37	8	5	0.9740	4.28	5.47
4	5	0.9647	4.92	6.34	9	5	0.9771	3.92	4.98
4	6	0.9636	5.00	6.40	10	4	0.9776	3.88	4.85
4	7	0.9641	5.12	6.52	20	5	0.9763	3.90	5.05

4.3 Evaluation Standards for the Developed Models

Several indicators were employed to assess the effectiveness of the suggested models, and the outcomes were computed using the equations provided. To ensure a comprehensive examination of a model's performance, it is crucial to apply multiple evaluation methodologies. A more thorough evaluation of the model's

capabilities and constraints is made possible by the use of a variety of metrics.

$$R^2 = \left(\frac{\sum_{i=1}^{N} (M_p - p')(M_a - a')}{\sqrt{\left[\sum_{i=1}^{N} (M_p - p')^2\right] \left[\sum_{i=1}^{N} (M_a - a')^2\right]}} \right)^2 \quad (22)$$

$$RMSE = \sqrt{\frac{\sum_{i=1}^{N} (M_a - M_p)^2}{N}} \quad (23)$$

$$MAE = \frac{\sum_{i=1}^{N} |M_P - M_a|}{N} \quad (24)$$

$$SI = \frac{RMSE}{p'} \quad (25)$$

$$OBJ = \left(\frac{n_{tr}}{n_{all}} \times \frac{RMSE_{tr} + MAE_{tr}}{R_{tr}^2 + 1} \right) + \left(\frac{n_{tst}}{n_{all}} \times \frac{RMSE_{tst} + MAE_{tst}}{R_{tst}^2 + 1} \right) \quad (26)$$

In the previous iterations, M_p and M_a represent the expected and actual route pattern values, respectively. The means of the actual and anticipated values are denoted by a′ and p′, respectively. The terms training datasets, tested datasets, and the number of patterns (collected data) in the connected dataset are represented by the letters t_r, t_{st}, and N, respectively. A model performs (badly) when the SI parameter is greater than 0.3, (reasonably) when it is between 0.2 and 0.3, (well) when it is between 0.1 and 0.2, and (excellently) when it is less than 0.1[42, 46].

5. Results and Analysis

5.1 The LR Model

Figure 4(a, b) illustrates the relationship between measured and predicted M_u for training and testing. The least squares and sum of error squares methods were used to determine the values of each parameter in the current model. An example of the LR model equation with various weight parameters is given by equation (27).

$$M_u = -51.99 + 0.08\,(b) + 0.26\,(h) - 0.08\,(f_c') + 17.33\,(\rho_s) + 11.38\,(\rho_f) + 0.02\,(E_{FRP}) \quad (27)$$

The beam overall height (h), steel reinforcement ratio (ρ_s), and FRP ratio (ρ_f) have the most influence on the M_u. This might be in line with the experimental results that have been published in the literature. The R^2, *RMSE*, and *MAE* assessment parameters for this model are, respectively, 0.79, 10.04, and 7.70 MPa. Additionally, as demonstrated in Section 6, the training dataset's *OBJ* and *SI* values for the current model are 6.93 and 0.21, respectively.

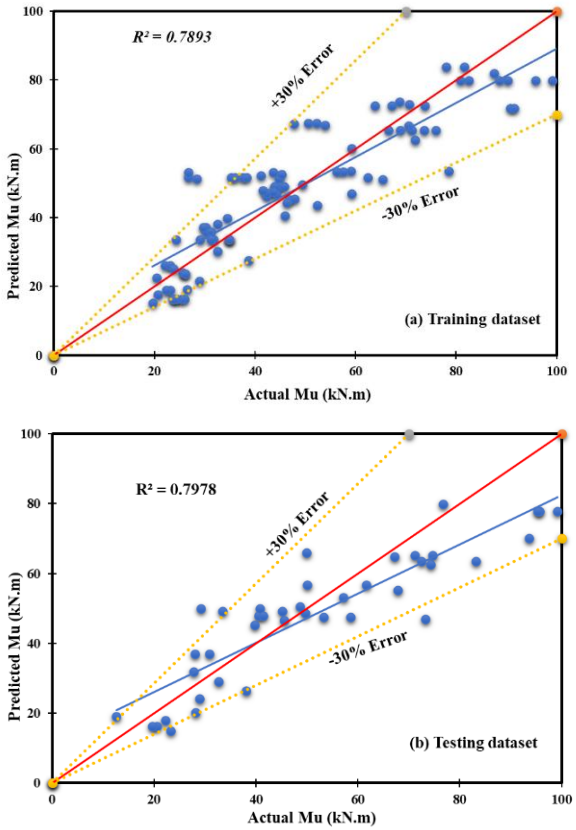

Figure 4: Comparison of the M_a that were tested and the M_p that the LR model predicted; (**a**): training datasets; (**b**): testing datasets.

5.2 NLR Model

As a training and testing dataset, Figure 5(a, b) illustrates the relation between predicted and actual M_u. The most significant factors that affect Mu are the overall depth of the beam (h), followed by the variation in the bottom flexural reinforcement (ρ_s). Equation (28) provides an NLR model formula with several variable parameters, states as follows:

$$M_u = -0.15 \times (b)^{0.12} \times (h)^{1.31} \times (f_c')^{-0.72} \times (\rho_s)^{0.95} \times (\rho_f)^{0.28} \times (E_{FRP})^{0.37} + 0.12 \times (b)^{0.26} \times (h)^{1.34} \times (f_c')^{-0.64} \times (\rho_s)^{0.80} \times (\rho_f)^{0.21} \times (E_{FRP})^{0.22} \quad (28)$$

The R^2, *RMSE*, and *MAE* values for this model are 0.88 MPa, 7.70 MPa, and 5.95 MPa, respectively. For the training dataset, the *OBJ* and *SI* values are 5.08 and 0.16, respectively.

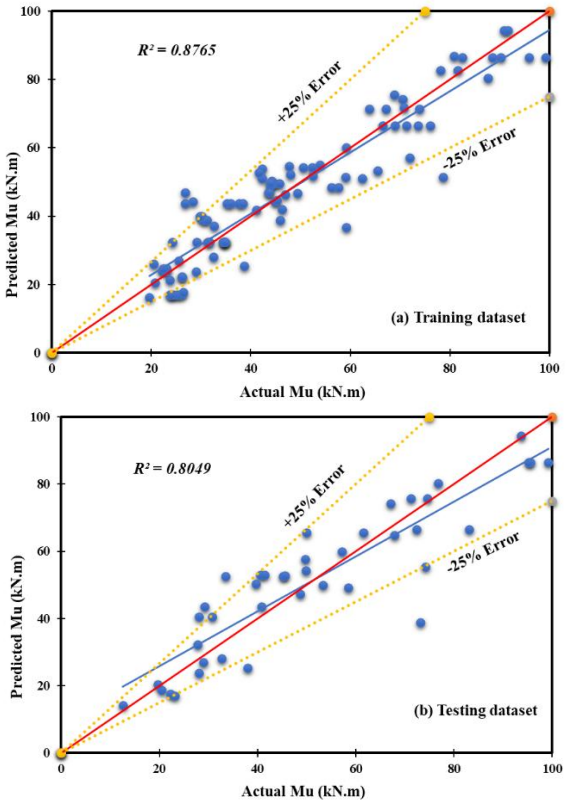

Figure 5: Comparison of the M_a that were tested and the M_p that the LR model predicted; (**a**) training datasets; (**b**) testing datasets.

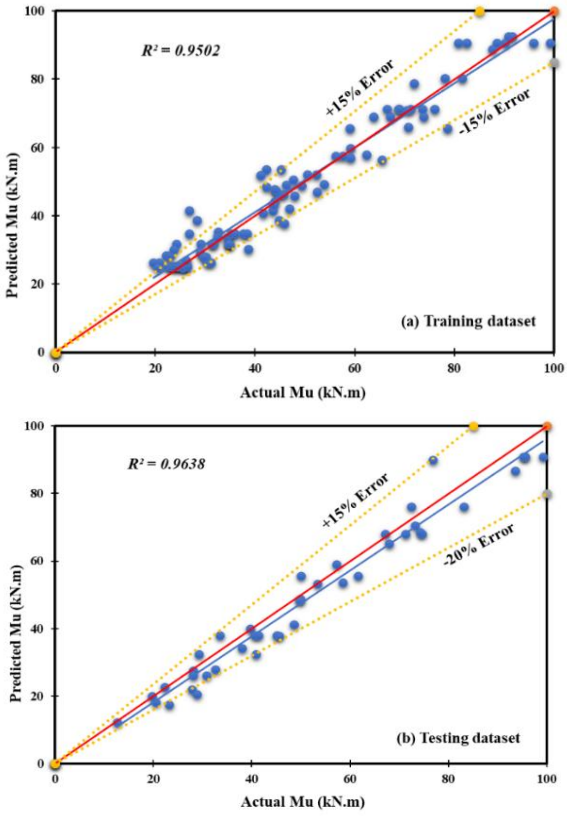

Figure 6: (**a**) A comparison between the tested M_a and the M_p predicted by the ANN model; (b) testing datasets.

5.3 ANN Model

Figure 6(a, b) compares the anticipated and actual Mu for training and testing datasets. The testing data has an error line of −20 percent and +15%, which is better than the other proposed models, compared to the training datasets' ±15% error line. R^2, RMSE, and MAE have respective assessment parameters of 0.95, 4.91, and 3.69. For the training set, the current model's OBJ and SI values are 3.08 and 0.10, respectively.

6. Comparison of Models

The flexural strength of the enhanced RC beam predicted by each model was evaluated using statistical indicators found in Section 5. The various ranges of prediction inaccuracy for every model, as illustrated in Figures 4, 5, 6, and 10, can be ascribed to variations in the modeling methodology and fundamental characteristics of each model. Compared to the NLR and LR models, which have error ranges of ±25% and ±30%, respectively, the ANN model has a smaller error range of ±15%. The reason for this difference can be attributed to the ANN model's outstanding ability to represent complex non-linear interactions, resulting in more accurate predictions. Furthermore, variables, including input characteristics, model complexity, and training data quality, affect each model's performance and could explain the observed variations in error ranges. Figures 7 through 9 illustrate how the ANN model performs in comparison to the LR and NLR. Its R^2 value is greater, while its RMSE and MAE values are lower. Model M_u predictions for strengthened RC beams based on testing datasets are shown in Figure 10. Figure 11 also displays the residual error for each model using the training and testing datasets. As can be seen from the comparable estimated and predicted M_u assessments for the model in Figures 12 and 13, the ANN model performs better than other models. Figure 12 shows the OBJ values for all developed models. The ANN, NLR, and LR models have values of 4.52 kN.m., 8.13 kN.m., and 10.34 kN.m., respectively. Compared to the NLR and LR models, the ANN model's OBJ value was 80% and 129% lower, respectively. This further demonstrates how the ANN model predicts the Mu more accurately for beams strengthened with FRP sheets.

Figure 13 displays the SI charge for the models that were provided for the training and testing procedures. It shows that, based on their performance as determined by the Scatter Index (SI) values, the three machine learning models LR, NLR, and ANN are compared in this study. The observed SI values for the data-trained set were 0.21 for LR, 0.16 for NLR, and 0.10 for ANN. On the other hand, it was discovered that the SI values for the data-tested set were 0.11 for ANN, 0.20 for NLR, and 0.23 for LR. Noteworthy SI values include 0 and 0.1, which denote excellent performance; 0.1 to 0.2, which denotes good performance; 0.2 to 0.3, which denotes fair performance; and 0.3 to 0.4, which denotes poor performance. In the data-tested set, the ANN and NLR models exhibited good performance based on these classifications, while the LR model performed fairly. During the training stage, in the testing phase, the ANN model's SI value is 109% lower than the LR model's, with a difference of 110%. Furthermore, compared to the NLR model, the ANN

model showed reduced SI values, with declines of 60% and 82% in training and testing, respectively. This comparison revealed that the ANN model can forecast the Mu of FRP-strengthened RC beams more competently and accurately than NLR and LR models.

In conclusion, it is important to note that any models with allowable errors can be utilized to predict the Mu of FRP-strengthened RC beams without the need for experimental programs. In addition, compared to other models, the ANN model can produce more precise results.

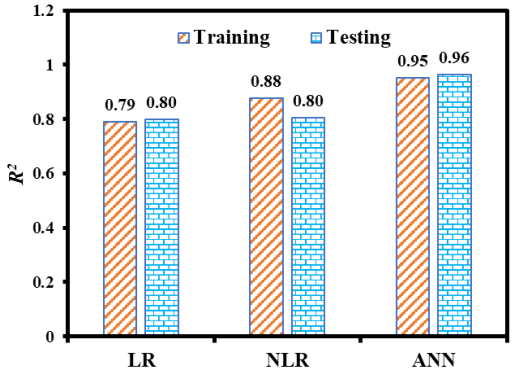

Figure 7: R^2 values for testing and training datasets for several models have been suggested.

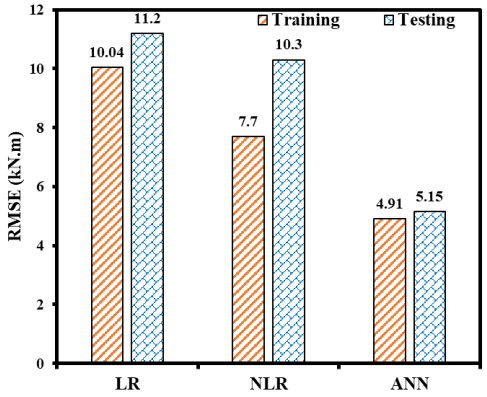

Figure 8: RMSE values for training and testing datasets for several models have been suggested.

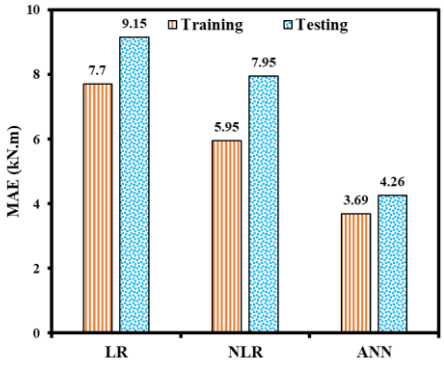

Figure 9: MAE findings for training and testing datasets for several models have been suggested.

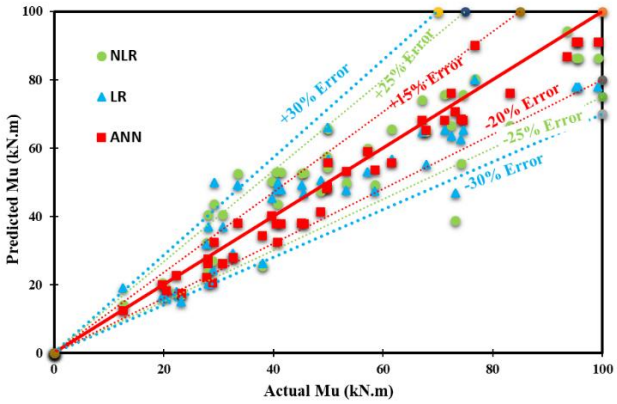

Figure 10: Analysis of the test dataset's model predictions in comparison.

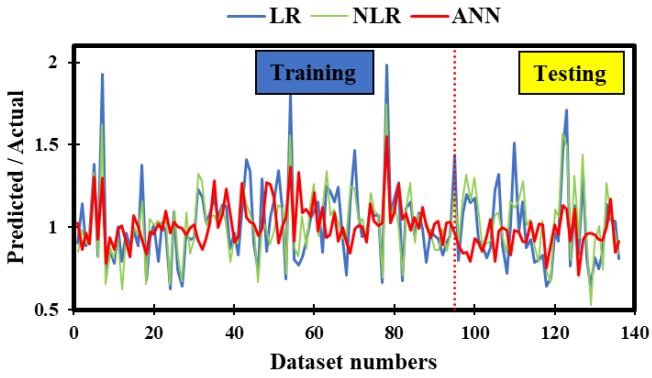

Figure 11: Mu residual error diagram that makes use of all available datasets for every model.

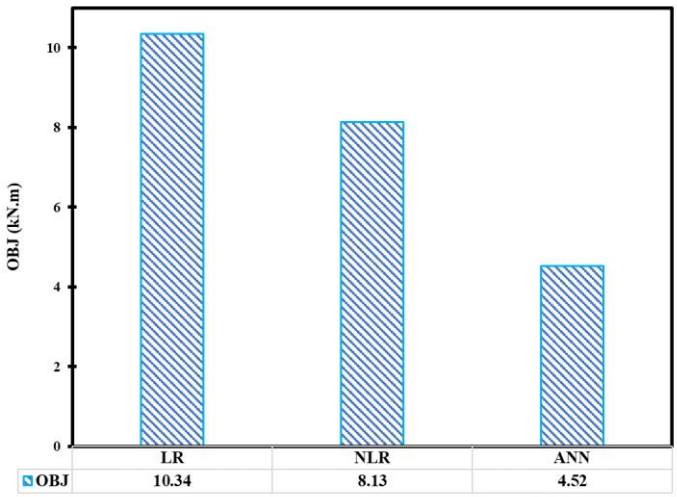

Figure 12: Every single model's OBJ value.

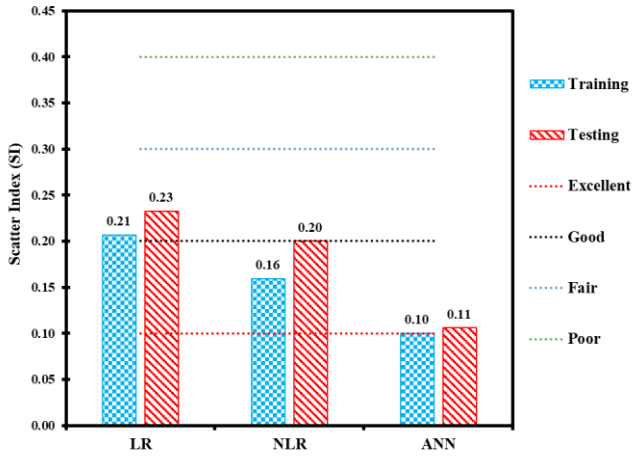

Figure 13: Results for all models' SI performance parameters.

7. Linear Correlation Matrix

The data in this study were analyzed using linear Pearson's correlation to assess the correlation between the variables. With coefficients of 0.83 and 0.17, respectively, it is clear that there is a substantial positive correlation between the flexural capacity of beams and the variables beam overall depth (h) and steel reinforcement ratio (ρ_s). A rise in h and ρ_s is correlated with an increase in flexural capacity, a pattern that is replicated in the basic ACI equation for beam flexural strength. Additionally, there is a fairly positive association between M and the FRP modulus (E_{FRP}). On the other hand, weak linear correlations are shown by $f'c$, ρ_f, and b, attributes indicating the existence of non-linear interactions between the inputs and the target variable. Table 4 provides a correlation matrix of coefficients.

Table 4: Correlation matrix among variables used in the development of models.

	b	h	$f'c$	ρ_s	ρ_f	E_{FRP}	M
b	1						
h	-0.15673	1					
$f'c$	-0.07142	-0.63563	1				
ρ_s	-0.27749	-0.1363	0.195893	1			
ρ_f	0.067765	-0.64163	0.598635	0.108475	1		
E_{FRP}	0.280745	0.047009	-0.17568	0.136703	-0.39686	1	
M	-0.04738	**0.833057**	-0.51335	**0.173179**	-0.46885	0.141059	1

8. Sensitivity and Parametric Analysis

The ANN model, which is more accurate than the LR and NLR models, was used to investigate the relationship between contributing parameters and flexural capacity. Analyzing each variable's relevance and contrasting the results with those of previous research are necessary steps in validating this model. As a result, a simulated dataset was created, as indicated in Table 5, in which one input variable was systematically changed between its extremes. In contrast, the others were kept constant at their mean values. The variance of the target variable was plotted against the input variable to determine the influence of a variable. Sensitivity analysis was also performed using the simulated dataset. Normalizing the difference in target variable values concerning each input variable allowed us to calculate the relative contribution of each contributing variable.

Table 5: Parametric and Sensitivity Analysis employing a simulated dataset.

Parameters	Range of Parameters	Number of Data Points	Constant Parameters
b (mm)	100 - 320	20	h=260mm; f'c=37MPa; ρ_s=0.75; ρ_f=0.29; E_{FRP}=151(MPa)
h (mm)	150 - 406	20	b=188mm; f'c=37MPa; ρ_s=0.75; ρ_f=0.29; E_{FRP}=151(MPa)
f'_c (MPa)	21 – 66.5	20	b=188mm; h=260mm; ρ_s=0.75; ρ_f=0.29; E_{FRP}=151(MPa)
ρ_s (%)	0.388 – 2.102	20	b=188mm; h=260mm; f'c=37MPa; ρ_f=0.29; E_{FRP}=151(MPa)
ρ_f (%)	0.04 – 1.205	20	b=188mm; h=260mm; f'c=37MPa; ρ_s=0.75; E_{FRP}=151(MPa)
E_{FRP} (MPa)	36 - 237	20	b=188mm; h=260mm; f'c=37MPa; ρ_s=0.75; ρf=0.29;

The results of the sensitivity analysis are shown in Figure 14. The sensitivity analysis results are consistent with Pearson's correlation values shown in Table 4. The most significant parameter among those examined in this study is the overall depth of the beam (h), followed by the variation in bottom flexural reinforcement (ρ_s). Furthermore, the flexural capacity of FRP-strengthened beams is determined in part by the width of the beam (b) and FRP ratio (ρ_f), both of which are considered important characteristics. On the other hand, the results indicate that the elastic modulus (E_{FRP}) and the concrete compressive strength ($f'c$) are the least important characteristics. Furthermore, upon examining ACI's flexural capacity formulas derived from mechanics principles (Equation (1)), it becomes evident that the nominal capacity is directly influenced by the effective depth and

steel reinforcement. As a result, the proposed model's results are in line with previous research, demonstrating the prediction model's validity for determining a beam's flexural capacity in the absence of observed data. The same results were obtained by others in the literature. Our results support the validity and dependability of our findings in the body of current literature because they are consistent with other studies[21].

The parametric analysis that was performed with the ANN model is shown in Figure 15. The bending capacity increases from 20 to 83 kN.m., indicating a change of 63 kN.m., as the beam depth increases from 155 to 387 mm. Similarly, a change of 26 kN.m is indicated by the increase in flexural capacity from 43 kN.m to 69 kN.m when the bottom reinforcement ratio is changed from 0.388 to 2.016. By changing the beam width from 100 to 320 mm, the bending capacity increases from 42 to 58 kN.m, which is a 16 kN.m change. Furthermore, there is a 15 kN.m enhancement in flexural capacity when the FRP ratio is changed from 0.04 to 1.14. The concrete's compressive strength and the FRP sheet's elastic modulus cause a difference in bending capacity of 4 and 2 kN.m., respectively. These results demonstrate the reliability of the created ANN model for future predictions and are in line with the outcomes of the sensitivity analysis and Pearson's correlation. The trained model is validated by the parametric study, which also makes sure that the trends detected by the ANN model and the trends in the literature are in line with each other.

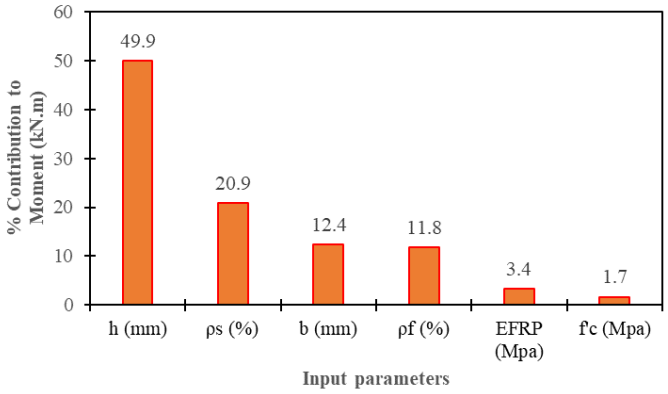

Figure 14: Contribution of the model parameters in predicting the M_u of strengthened RC beams.

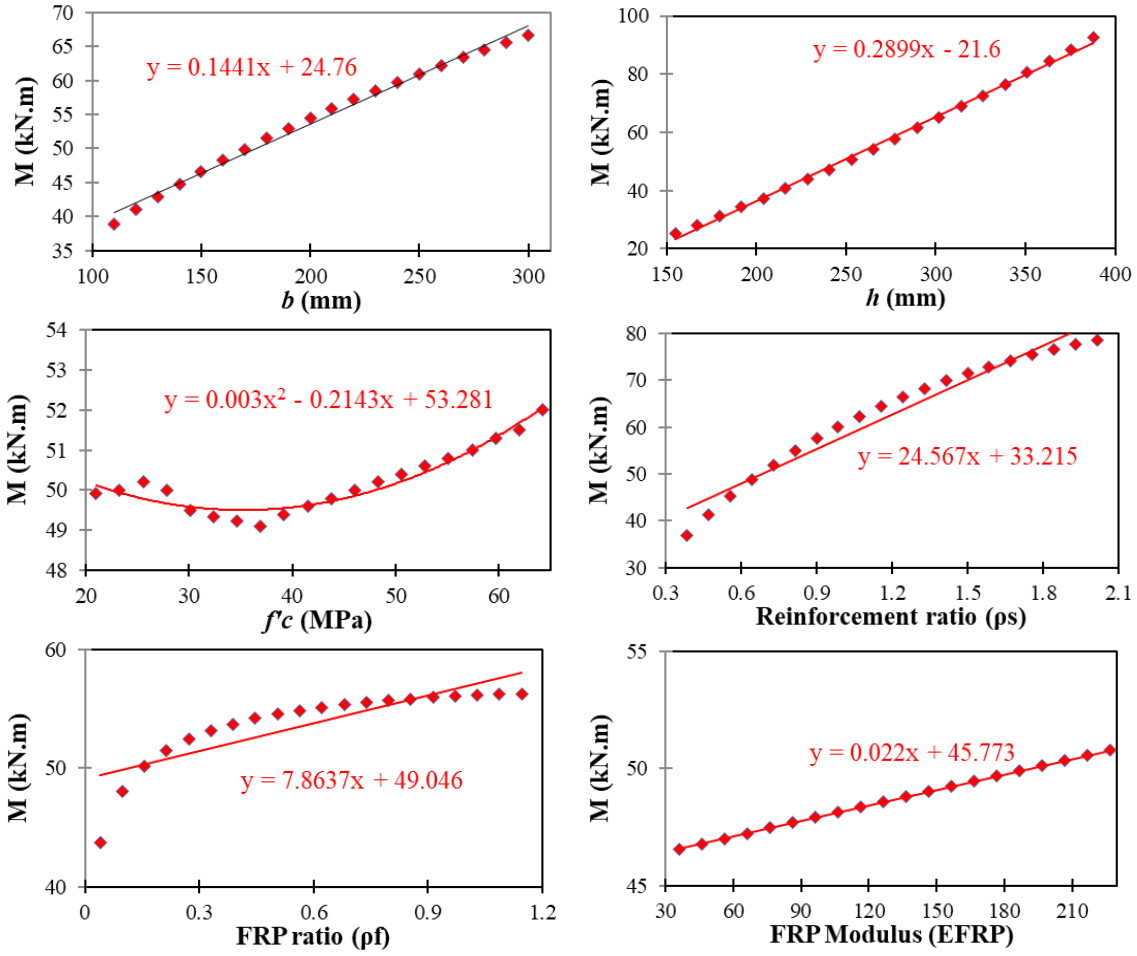

Figure 15: Parametric Analysis of the ANN Model

Conclusions

The current study demonstrated that when it comes to predicting the flexural behavior of reinforced concrete beams strengthened with fiber-reinforced polymer (FRP), Artificial Neural Networks (ANN) perform better than Non-linear Regression (NLR) and Linear Regression (LR) models. Our suggested ANN model performs satisfactorily; however, the availability of appropriate

data patterns affects the model's accuracy. Our suggested model shows promising results; however, there is a restricted number of research and patterns accessible in this particular field. More accurate and sophisticated models can be created over time with an increase in research. This work opens the door to more dependable structural engineering techniques by highlighting the potential of machine learning methods; specifically ANN, to improve the prediction accuracy of the flexural behavior of FRP-strengthened concrete beams.

1. The sensitivity analysis and statistical evaluation show that the ANN model performs better than the other two models. The model's R^2 values are 0.95 and 0.96 for the training and testing datasets, respectively. Furthermore, there are additional sensitivity indications for the RMSE, MAE, OBJ, and SI in the training dataset of the ANN model; the corresponding values are 4.91 MPa, 3.69 MPa, 4.52, and 0.10, respectively. As a result, the ANN model is more applicable and predictively accurate, making it appropriate for use in the preliminary design of the flexural strength of FPR-strengthened RC beams;

2. The estimated flexural strength of the FRP-strengthened RC beam was found to be between +15% and -20% of the measured flexural strengths for the training datasets, according to the ANN model. The rate for the remaining models was increased to ±30%;

3. A significant positive correlation was observed by Pearson's correlation analysis between the bending capacity and the overall depth of the beam (h) as well as the bottom flexural reinforcement (ρ_s). The results of the parametric and sensitivity analyses provided more evidence in favor of this observation. Furthermore, the ACI guidelines emphasized how important h and ρ_s are to improving the flexural capacity of the beams. Additionally, these factors had substantial contribution ratios: h contributed about 49.9%, and ρ_s contributed about 20.9% to the expected capacity, respectively. Furthermore, RC beam width (b) and the FRP ratio (ρ_f), which contributed 12.4% and 11.8%, respectively, had a moderate impact on capacity. On the other hand, the concrete compressive strength ($f'c$) and the FRP elastic modulus (E_{FRP}) had minimal impact.

The implementation of ANN models demonstrated promise in predicting the flexural behavior of concrete beams strengthened with fiber-reinforced polymer (FRP). In the future, research should look at different algorithms, such as genetic algorithms, as well as employ software like RapidMiner for superior evaluation and enhancement of models.

Conflict Of Interest

None

Author's Contributions

Nasih Habeeb Askandar: Literature review, data collection, data analysis, modeling, writing, reviewing, and editing.

Funding declaration

This paper did not receive any specific grant from funding agencies in the public, commercial, or not-for-profit sectors.

Acknowledgment

Authors express a great gratitude to Professor Ahed Khezam and Professor Hazem Melly for their big cooperation and help supporting this article.

References

1. Aslam, M., et al., *Strengthening of RC beams using prestressed fiber reinforced polymers–A review.* Construction and Building Materials, 2015. **82**: p. 235-256.
2. Kadhim, M.M., et al., *Review on NSM CFRP strengthened RC concrete beams in shear.* Advances in Civil Engineering, 2021. **2021**: p. 1-16.
3. Siddika, A., et al., *Strengthening of reinforced concrete beams by using fiber-reinforced polymer composites: A review.* Journal of Building Engineering, 2019. **25**: p. 100798.
4. Zhang, S.S., T. Yu, and G. Chen, *Reinforced concrete beams strengthened in flexure with near-surface mounted (NSM) CFRP strips: Current status and research needs.* Composites Part B: Engineering, 2017. **131**: p. 30-42.
5. Askandar, N. and A. Mahmood, *Comparative investigation on torsional behavior of RC beam strengthened with CFRP fabric wrapping and near-surface mounted (NSM) steel bar.* Advances in Civil Engineering, 2019. **2019**: p. 1-15.
6. Askandar, N.H. and A.D. Mahmood, *Torsional strengthening of RC beams with continuous spiral near-surface mounted steel wire rope.* International Journal of Concrete Structures and Materials, 2020. **14**(1): p. 7.
7. Habeeb Askandar, N. and A. Darweesh Mahmood, *Torsional Strengthening of RC Beams with Near-Surface Mounted Steel Bars.* Advances in Materials Science and Engineering, 2020. **2020**: p. 1-11.
8. Askandar, N.H., A.D. Mahmood, and R. Kurda, *Behavior of RC beams strengthened with FRP strips under the combined action of torsion and bending.* European Journal of Environmental and Civil Engineering, 2022. **26**(9): p. 4263-4279.
9. Bonacci, J. and M. Maalej, *Behavioral trends of RC beams strengthened with externally bonded FRP.* Journal of Composites for Construction, 2001. **5**(2): p. 102-113.
10. Hosen, M.A., et al., *Near-surface mounted composites for flexural strengthening of reinforced concrete beams.* Polymers, 2016. **8**(3): p. 67.
11. Seracino, R, et al., *Bond strength of near-surface mounted FRP strip-to-concrete joints.* Journal of Composites for Construction, 2007. **11**(4): p. 401-409.
12. Lorenzis, L.D. and A. Nanni, *Characterization of FRP rods as near-surface mounted reinforcement.* Journal of Composites for Construction, 2001. **5**(2): p. 114-121.
13. Le Hoang, T.T., et al., *An artificial neural network for predicting the ultimate bending moments in reinforced concrete beams with fiber-reinforced polymer strengthening.* Asian Journal of Civil Engineering, 2023: p. 1-11.
14. Thai, H.-T. *Machine learning for structural engineering: A state-of-the-art review*. In *Structures*. 2022. Elsevier.
15. Izadgoshasb, H, et al., *Predicting compressive strength of 3D printed mortar in structural members using machine learning.* Applied Sciences, 2021. **11**(22): p. 10826.
16. Kandiri, A, et al., *Modified Artificial neural networks and support vector regression to predict lateral pressure exerted by fresh concrete on formwork.* International Journal of Concrete Structures and Materials, 2022. **16**(1): p. 1-22.

17. Yousif, S.T. and M. A AL-Jurmaa, *Modeling of ultimate load for RC beams strengthened with Carbon FRP using artificial neural networks.* Al-Rafidain Engineering Journal (AREJ), 2010. **18**(6): p. 28-41.
18. ACI440.2R-08, *Design and Construction of Externally Bonded FRP Systems for Strengthening Concrete Structures*. 2008, American Concrete Institute: Farmington Hills, MI, U.S.A.
19. Xue, W., Y. Tan, and L. Zeng, *Flexural response predictions of reinforced concrete beams strengthened with prestressed CFRP plates.* Composite Structures, 2010. **92**(3): p. 612-622.
20. Al-Mahmoud, F, et al., *Strengthening of RC members with near-surface mounted CFRP rods.* Composite structures, 2009. **91**(2): p. 138-147.
21. Khan, K, et al., *Estimating flexural strength of FRP reinforced beam using artificial neural network and random forest prediction models.* Polymers, 2022. **14**(11): p. 2270.
22. Hu, T. and G. Li, *Machine Learning-based model in predicting the plate-end debonding of FRP-strengthened RC beams in flexure.* Advances in Civil Engineering, 2022. **2022**.
23. Arduini, M. and A. Nanni, *Behavior of precracked RC beams strengthened with carbon FRP sheets.* Journal of composites for construction, 1997. **1**(2): p. 63-70.
24. Rahimi, H. and A. Hutchinson, *Concrete beams strengthened with externally bonded FRP plates.* Journal of composites for construction, 2001. **5**(1): p. 44-56.
25. Breña, S.F., et al., *Use of carbon fiber reinforced polymer composites to increase the flexural capacity of reinforced concrete beams*. 2001, University of Texas at Austin.
26. Barros, J.A. and A. Fortes, *Flexural strengthening of concrete beams with CFRP laminates bonded into slits.* Cement and Concrete Composites, 2005. **27**(4): p. 471-480.
27. Soliman, S.M., E. El-Salakawy, and B. Benmokrane, *Flexural behavior of concrete beams strengthened with near surface mounted fiber reinforced polymer bars.* Canadian Journal of Civil Engineering, 2010. **37**(10): p. 1371-1382.
28. Nakul, R., *Static and impact load response of reinforced concrete beams and slabs with NSM-CFRP retrofitting.* 2012, Norfolk: Old Domin**-** ion University.
29. Sharaky, I.A., et al., *Flexural response of reinforced concrete (RC) beams strengthened with near surface mounted (NSM) fiber reinforced polymer (FRP) bars.* Composite Structures, 2014. **109**: p. 8-22.
30. Al-Obaidi, S., *Behavior of reinforced concrete beams retrofitted in flexure using CFRP-NSM technique.* 2015.
31. Seo, S.-y., et al., *Flexural strength of RC beam strengthened by partially de-bonded near surface-mounted FRP strip.* International Journal of Concrete Structures and Materials, 2016. **10**(2): p. 149-161.
32. Daghash, S.M, and O.E. Ozbulut, *Flexural performance evaluation of NSM basalt FRP-strengthened concrete beams using digital image correlation system.* Composite Structures, 2017. **176**: p. 748-756.
33. Jung, W.-t., et al., *Flexural behavior of concrete beam strengthened by near-surface mounted CFRP reinforcement using equivalent section model.* Advances in Materials Science and Engineering, 2017. **2017**.
34. Trung, T.L.H., et al., *Study on performance of reinforced concrete beams strengthened with carbon fiber strands under impact.* Journal of Structural Engineering, A, 2018. **64**: p. 865-874.
35. Moawad, M.A.M.M., *Flexural behavior of NSM FRP strengthened reinforced concrete beams under sustained loading.* 2020.
36. Liu, D, et al., *Flexural behavior of reinforced concrete (RC) beams strengthened with carbon fiber reinforced polymer (CFRP) and ECC.* Case Studies in Construction Materials, 2023. **19**: p. e02270.
37. ACI440.2R-17, *Design and Construction of Externally Bonded FRP Systems for Strengthening Concrete Structures*. 2017, American Concrete Institute: Farmington Hills, MI, U.S.A.
38. ACI318M-19, *Building Code Requirements for Structural Concrete, American Concrete Institute*. 2019, American Concrete Institute: Farmington Hills, MI, USA.
39. ACI318M-5, *Building Code Requirements for Structural Concrete, American Concrete Institute*. 2005, American Concrete Institute: Farmington Hills, MI, USA.
40. Yu, K., J. Yu, and Z. Lu. *Mechanical characteristics of ultra-high performance strain-hardening cementitious composites*. In *Strain-Hardening Cement-Based Composites: SHCC4 4*. 2018. Springer.
41. Qadir, W., K. Ghafor, and A. Mohammed, *Characterizing and modeling the mechanical properties of the cement mortar modified with fly ash for various water-to-cement ratios and curing times.* Advances in Civil Engineering, 2019. **2019**.
42. Ghafor, K, et al., *Computing models to predict the compressive strength of engineered cementitious composites (ECC) at various mix proportions.* Sustainability, 2022. **14**(19): p. 12876.
43. Quinlan, J.R. *Learning with continuous classes*. In the *5th Australian Joint Conference on Artificial Intelligence*. 1992. World Scientific.
44. Malerba, D., et al., *Top-down induction of model trees with regression and splitting nodes.* IEEE Transactions on Pattern Analysis and Machine Intelligence, 2004. **26**(5): p. 612-625.
45. Askandar, N.H, G.B. Jumaa, and G.H. Ahmed, *Modeling for torsional strength prediction of strengthened RC beams.* Multiscale and Multidisciplinary Modeling, Experiments and Design, 2024: p. 1-19.
46. Li, M.-F., et al., *General models for estimating daily global solar radiation for different solar radiation zones in mainland China.* Energy conversion and management, 2013. **70**: p. 139-148.